ACS APPLIED MATERIALS & INTERFACES

RESEARCH ARTICLE

www.acsami.org

Photoelectrochemical and Photocatalytic Properties of Biphasic Organic p- and n-Type Semiconductor Nanoparticles Fabricated by a Reprecipitation Process

Shuai Zhang,[†,‡] Ryohei Sakai,[†] Toshiyuki Abe,[§] Tomokazu Iyoda,[†] Takayoshi Norimatsu,[‡] and Keiji Nagai*[,†]

[†]Division of Integrated Molecular Engineering, Chemical Resources Laboratory, Tokyo Institute of Technology, Yokohama 226-8503, Japan

[§]Department of Frontier Materials Chemistry, Graduate School of Science and Technology, Hirosaki University, 3 Bunkyo-cho, Hirosaki, Aomori 036-8561, Japan

[‡]Division of Energetic Materials for Photonics, Institute of Laser Engineering, Osaka University, Suita 565-0871, Japan

Supporting Information

ABSTRACT: The visible-light-responsive photoelectrochemical and photocatalytic properties of nanoparticles of C_{60}, partially hydrolyzed aluminum phthalocyanine chloride (denoted as AlPc), and a composite of the two are reported. The three types of nanoparticles were obtained through a reprecipitation method from *N*-methyl-2-pyrrolidone solutions of C_{60}, aluminum phthalocyanine chloride (AlPcCl), and their mixture, respectively. The nanoparticle composite's ultraviolet−visible absorption, diffuse-reflectance and Fourier transform IR spectra, X-ray diffraction pattern, and scanning electron microscopy image are all similar to the sum of those of the C_{60} and AlPc particles, respectively. The nano-ordered composite exhibits p/n junctionlike photoelectrochemical characteristics, which were investigated in comparison with those of vapor-deposited C_{60} (n-type), AlPcCl (p-type), C_{60}/AlPcCl (n/p), and AlPcCl/C_{60} (p/n) electrodes. The nanoparticle composite further shows photocatalytic activity for the decomposition of trimethylamine to carbon dioxide in a suspension system.

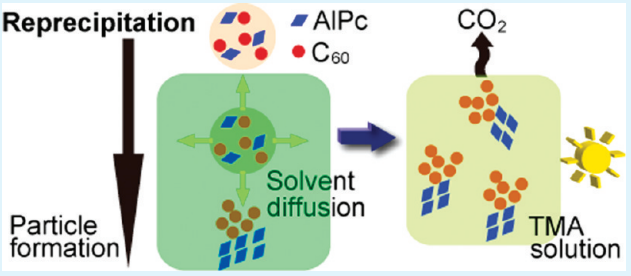

KEYWORDS: photoanodic current, visible-light-responsive photocatalyst, trimethylamine, photochemistry, reprecipitation

INTRODUCTION

Organic semiconductors with heterojunctions have been widely used to construct low-cost and high-efficiency photoenergy conversion systems in the dry state[1−14] or to sensitize inorganic semiconductors in the liquid phase.[15−21] However, only a few studies have investigated the application of organic semiconductors to photocatalysis, for instance, carbond dioxide (CO_2) photofixation[22−25] and water splitting,[26,27] in which the heterojunction structure was not utilized despite its importance for achieving highly efficient charge separation. Recently, Abe and co-workers investigated the photoelectrochemistry of organic p/n bilayers of phthalocyanine and fullerene C_{60} or a perylene derivative in the water phase[28−34] and achieved water splitting under visible light and small bias.[28,31,34] The studies indicate that photoinduced redox reactions occur catalytically on the semiconductor surfaces and that the organic bilayers of the p/n junction lead to an efficient generation of photocurrent in comparison with the single layers of the Schottky junction. Furthermore, a p/n junction was also utilized for a laser-induced reflection device without electrode contacts to control laser ablation.[35,36] These examples indicate that organic p/n junctions can be applied not only to solar cells but also to other devices without electrodes. On the basis of these reports, we applied an organic n/p bilayer of a perylene derivative and metal-free phthalocyanine (H_2Pc) coated on a Nafion membrane for the photodegradation of organic pollutants,[37] wherein the organophotocatalyst was highly responsive to visible light.

The fabrication cost of the above-mentioned photocatalyst with a p/n junction is high because of the dry process (i.e., vapor deposition) and the use of Nafion. It is therefore necessary to develop a new organic photocatalyst with low fabrication cost for practical use. The reprecipitation method reported by Kasai and co-workers[38−47] offers a potential pathway. This method is a wet process suitable for the preparation of various organic crystals whose sizes range from nanometers to micrometers in order to develop electronic and photonic devices. For example, some nanocrystals exhibited a blue shift of the absorption bands upon decreased crystal size,[42,43] similar to the quantum confinement effect observed in metal and inorganic semiconductor nanocrystals, although the size range for the effect is about an order of magnitude larger in the case of organic nanocrystals. However, to the best of our knowledge, studies on the photocatalytic characteristics of organic nanocrystals composed of both p- and n-type semiconductors have not yet been reported.

Organic dye clusters consisting of fullerene and porphyrin[15−19,21] have already been introduced by Imahori, Fukuzumi, Kamat, and

Received: January 25, 2011
Accepted: May 23, 2011
Published: May 23, 2011

their co-workers through reprecipitation, as sensitizers of inorganic semiconductors in solar cells. These clusters have units of donor−acceptor (D−A) pairs and only one kind of crystalline structure—D−A supramolecular crystalline[17]—because of the charge-transfer interaction between the donor and acceptor in a nonpolar solvent.

Herein, we report the preparation of an organic nanoparticle composite with two types of crystalline structures—n-type C_{60} and p-type partially hydrolyzed aluminum phthalocyanine chloride (denoted hereafter as AlPc)[48] crystals—through reprecipitation from a polar solvent. In addition to characterizing the resulting composite by ultraviolet−visible (UV−vis), diffuse-reflectance and Fourier transform infrared (FTIR) spectroscopies, X-ray diffraction (XRD), and scanning electron microscopy (SEM), we investigated its photoelectrochemical properties in comparison with the monocomponent nanoparticles of n-type C_{60} and p-type AlPc. Furthermore, we also investigated its photocatalytic property in terms of decomposing trimethylamine (TMA) to CO_2 under visible-light irradiation.

EXPERIMENTAL SECTION

Materials. Fullerene C_{60} (99%) was obtained from Tokyo Chemical Industry Co., Ltd. (TCI), and used as received. Aluminum phthalocyanine chloride (AlPcCl, TCI) was purified twice by sublimation prior to use. An indium−tin oxide (ITO)-coated glass plate (resistance, 8 Ω/cm^2; transmittance, >85%; ITO thickness, 174 nm) was commercially available from Asahi Glass Co., Ltd., and was washed by sonication in water-containing detergent, pure water, acetone, and ethanol in that sequence. The ITO plate was dried in air before use. All other solvents and chemicals were of reagent-grade quality, were purchased commercially, and were used without further purification.

Preparation of Particles. AlPcCl and C_{60} were soluble in *N*-methyl-2-pyrrolidone (NMP) and insoluble in water. The C_{60}, AlPc, or composite particles were prepared by first dissolving 34.4 mg of C_{60} and/or 34.4 mg of AlPcCl in 40 mL of NMP solvent. This solution was then injected into 400 mL of water by a syringe pump with an agitation rate of 750 rpm and an injection rate of 5 mL/min (volume ratio of NMP to water = 1:10). After injection, the solution was kept stirring for 30 min to form a suspension. Successively, a required amount of the suspension was mixed with a 1 M HCl aqueous solution (volume ratio of HCl solution to suspension = 1:100), and the suspension was kept overnight in order to collect particles by filtration [hydrophilic poly(tetrafluoroethylene) membrane, pore size 0.2 μm], in which NMP and HCl were removed by a gentle washing with water. Finally, the particles on the membrane were dried in a vacuum at 60 °C or redispersed in pure water by sonication for characterization and other experiments. Simply mixed particles were prepared by mixing particles of C_{60} with those of AlPc (weight ratio = 1:1), whereas the nanoparticle composite was prepared by reprecipitation of the mixed NMP solution of C_{60} and AlPcCl.

Characterization. UV−vis absorption spectra of solutions and suspensions were recorded by a Shimadzu UV-3100s. Diffuse-reflectance spectra of dried particles were also measured by the Shimadzu UV-3100s with samples spread on $BaSO_4$ plates. FTIR spectra were recorded in a KBr pellet using a Jasco FTIR-660 Plus. The morphology of different particles was observed by SEM measurements using a JEOL JSM 7400 FS. XRD measurements were performed on a Rigaku Rint Ultima+ diffractometer using Cu Kα radiation.

Photoelectrochemical Measurements. All of the photoelectrochemical measurements were carried out in a standard three-electrode system, which was equipped with a modified ITO working electrode, a Pt wire counter electrode, and an Ag/AgCl (in a saturated KCl electrolyte) reference electrode, using a cyclic voltammetry (CV) tool (Hokuto Denko HSV-100). Working electrodes were prepared by casting the suspensions and drying at room temperature. For instance, 0.15 mL of a 0.1 mg/mL suspension was cast on an ITO electrode with an effective area of 1 cm^2. The working electrode was contacted with a 0.1 mol/L KNO_3 solution containing 2×10^{-3} mol/L TMA in a dinitrogen atmosphere for investigating photoanodic characteristics. A halogen lamp was used as the light source, and light was illuminated on the working electrode from the ITO side. The light intensity, which was 100 mW/cm^2, was monitored and corrected using an optical power meter (3A-SH, Ophir, Ltd.).

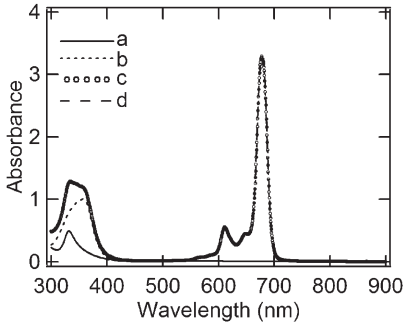

Figure 1. Absorption spectra of (a) C_{60} (8.6×10^{-3} mg/mL) (—), (b) AlPcCl (8.6×10^{-3} mg/mL) (●), and (c) a mixture of AlPcCl and C_{60} (8.6×10^{-3} mg/mL, respectively) (○) dissolved in NMP. (d) Sum of lines a and b (- - -). Lines c and d overlap completely; the overlap between lines b and c/d covers ~400−900 nm.

The internal quantum efficiency (IQE) spectrum for the photoanodic current was measured using a halogen lamp (150 W) as the light source in combination with a monochromator (SG-100, Kohken Co., Ltd.). The incident photon number intensity was adjusted to 3.5×10^{13} cm^{-2} s^{-1} at each wavelength and monitored by the power meter. In this experiment, an electrolyte containing 1×10^{-2} mol/L TMA and 0.1 mol/L KNO_3 was used within an argon atmosphere. The IQE was calculated by the following equation:

$$\text{IQE}\ (\%) = \{[I/e]/[W(1 - 10^{-A})/\varepsilon]\} \times 100 \qquad (1)$$

where I (A/cm^2) is the photocurrent density, e (C) is the elementary electric charge, W (W/cm^2) is the monochromatic light intensity, A is the absorbance of the composite nanoparticles on the electrode, and ε is the photon energy.

Photocatalytic Degradation of TMA. The photocatalytic activity of the resulting particles was evaluated by photodegradation of TMA in water. In the test, 2 mg of the powdered catalyst was first dispersed in 2 mL of pure water by sonication, after which an aqueous solution of concentrated TMA was added to adjust the TMA concentration to 20 ppm. Subsequently, the reaction solution was enclosed in a cylindrical Pyrex cell (5 mL, external diameter 16.5 mm, and height 45 mm), and the particles were dispersed with stirring during the reaction. The reactor was then irradiated with visible light, where a 500-W halogen lamp was used as the light source in combination with a cutoff filter (L-42, Hoya Corp.) for UV light and a water cutoff filter for IR light, in particular to keep the reactor at room temperature. The light intensity was 23 mW/cm^2, which was monitored and corrected by the optical power meter. The irradiation area was about 3.5 cm^2. After 40 h of irradiation, the amount of CO_2 generated was detected by a flame ionization detector attached to a gas chromatograph (GC-2014, Shimadzu Co., Ltd.) equipped with a Porapak N column and a methanizer (MTN-1, Shimadzu Co., Ltd.).

RESULTS AND DISCUSSION

Characterization of C_{60}, AlPc, and Composite Particles. The absorption spectra of solutions of AlPcCl, C_{60}, and their mixture in NMP are shown in Figure 1. The spectrum of AlPcCl in the solution (line b in Figure 1) has a strong Q-band absorption with a peak at 680 nm,[12] and that of C_{60} (line a in Figure 1) exhibits a

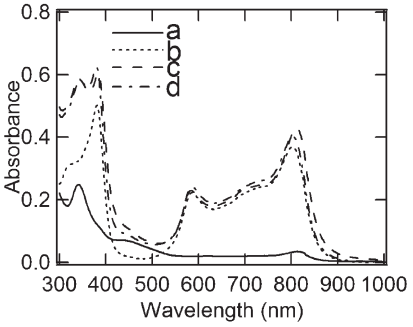

Figure 2. Absorption spectra of particle suspensions of (a) C_{60} (8.6×10^{-4} mg/mL) (—), (b) AlPc (8.6×10^{-4} mg/mL) (●), and (c) composite (1.72×10^{-3} mg/mL) (- - -). (d) Sum of lines a and b (-·-). The composite's loading mole ratio of AlPcCl to C_{60} was 5:4.

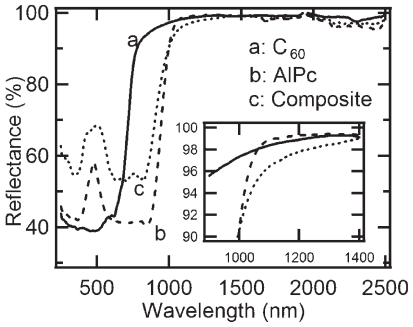

Figure 3. Diffuse-reflectance spectra of different particles of (a) C_{60} (—), (b) AlPc (- - -), and (c) composite (●). The inset shows an expansion of the 1000−1400 nm region. The composite's loading mole ratio of AlPcCl to C_{60} was 5:4.

characteristic peak at 340 nm.[49] For the mixed solution of C_{60} and AlPcCl (line c in Figure 1), absorption bands appear without any shift or intensity change compared to the arithmetical sum of the spectra of C_{60} and AlPcCl (line d in Figure 1), suggesting that C_{60} and AlPcCl do not form a charge-transfer complex in NMP.

Here, the composite suspension denotes that containing the particles obtained through reprecipitation from the mixed solution of C_{60} and AlPcCl in NMP. The absorption spectra of the C_{60}, AlPc, and composite suspensions in a NMP/water mixture (lines a−c in Figure 2) were compared with those of the original NMP solutions (lines a−c in Figure 1), respectively. In each case, the absorption band of the suspension is broader than that of the corresponding NMP solution. This broadening is indicative of nanoparticle formation in the NMP/water mixture.[47] Similar broadening has also been reported for porphyrin[21] and fullerene[50] aggregation. In addition, the absorption spectrum of the composite suspension (line c in Figure 2) has a structure similar to that of the sum of the absorption spectra of C_{60} and AlPc in a NMP/water mixture (line d in Figure 2). This indicates that the composite suspension consists of both C_{60} particles and AlPc particles.

By means of diffuse-reflectance spectroscopy, it is observed that the light absorption of the composite (line c in Figure 3) covers the entire visible light region and further extends to the near-IR region, indicating that the composite has the potential to respond to the full spectrum of visible light. In addition, it also has a slight broadening around the wavelength of 1200 nm in comparison with the spectra of the monocomponent particles of C_{60} and AlPc, as shown in the inset of Figure 3.

To evaluate the shapes and morphologies of the particles prepared by reprecipitation, SEM measurements were performed. The C_{60} particles are spherical crystals polydispersed in size (90 nm on average; Figure 4A). Their morphology is different from Kasai et al.'s hexagonal multibranched C_{60}·two thirds *m*-xylene micro/nanocrystals;[40] this difference is related to the different supersaturation ratios. The supersaturation ratio is a key parameter for understanding the crystallization mechanism of organic nanoparticles;[51] it is defined as C/C_e, where C is the initial target compound concentration in a good solvent and C_e is the solubility of the target compound in a poor solvent. At high supersaturation ratios, molecules aggregate rapidly, and crystal growth occurs at a higher rate through aggregation of the nucleated particles. Considering that the solubility of C_{60} in 2-propanol (Kasai et al.'s case), a poor solvent, is about 1.6×10^8 times as large as that in water (the present case),[52] the crystallization rate in water must be much higher than that in 2-propanol. Besides the supersaturation ratio, interaction between the target compound and solvent can also affect the nucleation process; this phenomenon has been observed for the micro- and nanostructural growth of the low-density polymer foams in wet processes.[53,54] For the present case, it has been reported that C_{60}−NMP interaction induces a slow aggregation process of C_{60} in its NMP solution under near-saturation concentrations.[55] This may also be related to the morphological differences between the present C_{60} nanoparticles and the C_{60}·two thirds *m*-xylene micro/nanocrystals.

The AlPc particles obtained here are platelike with an average size of 70 nm (Figure 4B). In the case of previous research on the alkyl-substituted phthalocyanine clusters of octaalkoxyphthalocyanine (C_8Pc) reported by Imahori and co-workers,[20] the long alkyl chains of C_8Pc were important for increasing the solubility of phthalocyanine in toluene and necessary for the formation of clusters in the toluene/acetonitrile mixture. In our experiments, platelike nanoparticles were formed using alkyl chain-free phthalocyanine. This may be ascribed to the use of water, an extremely poor solvent, similar to the above-mentioned case of C_{60}. The platelike morphology of the AlPc nanoparticles may also be due to the stacking of AlPc molecules along the axis perpendicular to the molecular plane.

It is noteworthy that the nanoparticle composite contains both spherical (indicated by circles) and platelike (indicated by rectangles) particles with an average size of 20 nm. The size is much smaller than that of the C_{60} or AlPc particles, as shown in Figure 4C,D. The existence of at least two morphologies is consistent with the similarity between the UV−vis absorption spectrum of the composite suspension (line c in Figure 2) and the sum of the C_{60} and AlPc suspension spectra (line d in Figure 2). For one example of D−A complex nanoclusters composed of C_8Pc and perylenediimide,[20] the morphology was quite different from that of C_8Pc or perylenediimide nanoclusters: in the details, the perylenediimide molecules were considered to be incorporated into the C_8Pc aggregates to form larger clusters with a supramolecular structure. The structural difference between the present nanoparticle composite and the D−A complex nanoclusters arises from the differences in their preparation. In the preparation of the present composite, a polar solvent, NMP, was used to dissolve AlPcCl and C_{60}, resulting in a weaker D−A interaction than that in the case of a nonpolar solvent, toluene, used to dissolve C_8Pc and perylenediimide.[20] Thus, the present composite would be solidified separately. The faster nucleation and rate of crystal growth described above might also account for the smaller and multiphasic crystals.

The crystalline phase of the composite was identified by XRD. Diffraction peaks of C_{60} and AlPc crystallites are shown in Figure 5. The peaks at 2θ = 10.9°, 16.9°, 20.6°, 21.4°, 27.4°,

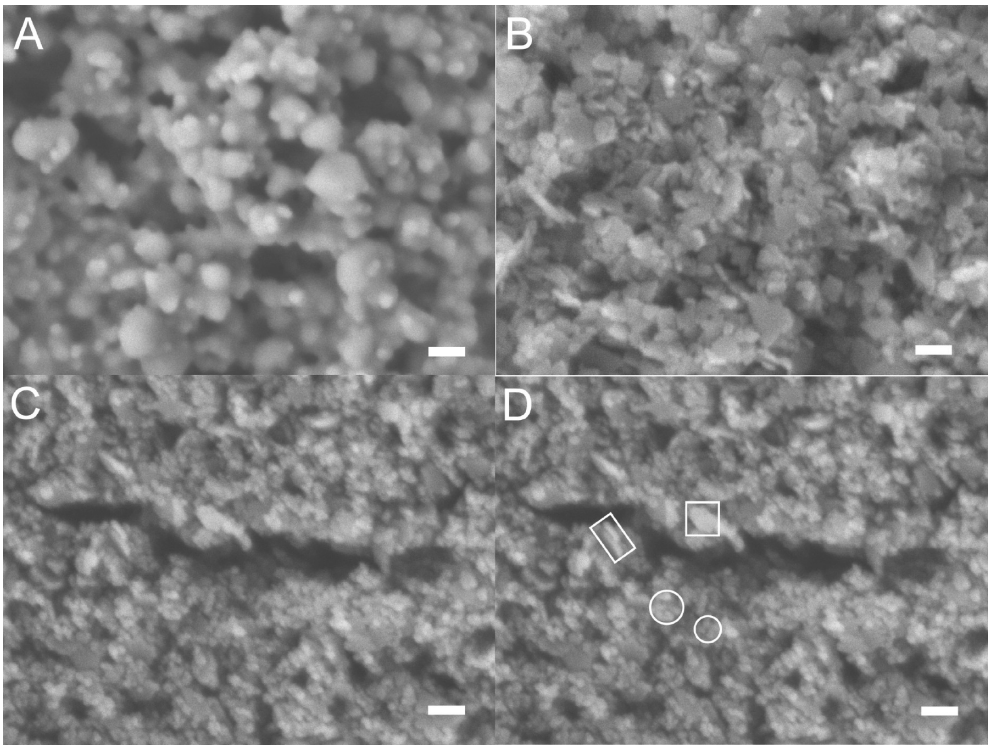

Figure 4. SEM images of different particles of (A) C_{60}, (B) AlPc, and (C and D) composite. Panel D is the same as panel C except for the indicators (circles and rectangles). The composite's loading mole ratio of AlPcCl to C_{60} was 5:4. The magnitude of the scale bars represents 100 nm for all images.

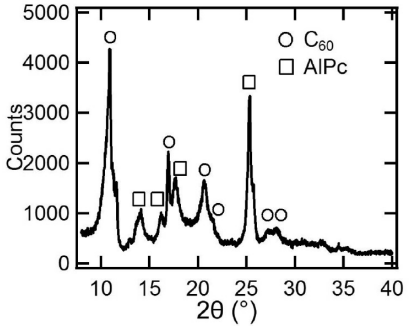

Figure 5. XRD pattern of the nanoparticle composite. The peaks from C_{60} and AlPc are marked with circles and squares, respectively. The composite's loading mole ratio of AlPcCl to C_{60} was 5:4.

and 28.1° were indexed as the (111), (220), (311), (222), (331), and (420) planes of face-centered-cubic pristine C_{60}.[56,57] The intense peak at $2\theta = 25.3°$, which corresponds to a d spacing of 3.5 Å, is near the position of the characteristic diffraction peak for pristine AlPcCl at $2\theta = 27°$.[58,59] This can be explained by the partial hydrolysis of AlPcCl to AlPcOH,[58] which is also supported in terms of the FTIR spectra (Figure S1 in the Supporting Information). Therefore, the partially transformed p-type semiconductors and p-type nanoparticles are collectively referred to as AlPc and AlPc nanoparticles, respectively. The XRD data identify two crystalline structures—both C_{60} and AlPc—in the composite.

Photoelectrochemical Characteristics of Particles on ITO. According to the diffuse-reflectance spectra, SEM images, and XRD pattern, there are two crystalline components—C_{60} and AlPc—in the composite. This implies the existence of physical contact between them, which may possess p/n junction characteristics to achieve efficient charge separation at the C_{60}/AlPc interface. In order to investigate this, photoelectrochemical measurements were carried out that have also been used to characterize the p/n junction of vapor-deposited C_{60} and H_2Pc bilayers in the previous studies.[30,33] The studies indicate that the photocurrent of the p/n bilayer involves charge separation at the p/n junction and subsequent carrier consumption at the solid/liquid interface, whereas that of the monolayer is based on the characteristics of a semiconductor/liquid junction (i.e., Schottky junction). The photoelectrochemical processes of the organic semiconductors in the presence of an electron donor are shown in Figure 6.

Vapor-deposited electrodes composed of C_{60} and/or AlPcCl were prepared and first studied as a reference of the nanoparticles. As shown in Figure S2 in the Supporting Information, the vapor-deposited bilayers also show the photoelectrochemical characteristics of p/n junction according to the schemes in Figure 6c, d. In the presence of TMA, which is chosen as the electron donor, photoanodic currents are observed only for ITO/C_{60}/AlPcCl (n/p; Figure S2c in the Supporting Information) and ITO/C_{60} (n-type; Figure S2a in the Supporting Information), both of which have the threshold potential of ∼−0.2 V vs Ag/AgCl. Another bilayer electrode of ITO/AlPcCl/C_{60} (p/n; Figure S2d in the Supporting Information) does not show a photoanodic current, while ITO/AlPcCl (p-type; Figure S2b in the Supporting Information) shows anodic current as +0.4 V vs Ag/AgCl, whose threshold potential is more positive, and the resulting current is independent of light illumination. The large photoanodic current observed for the ITO/C_{60}/AlPcCl bilayer is evidently different from that for the AlPcCl monolayer and similar to that for the reported n/p bilayer electrode of ITO/C_{60}/H_2Pc,[30] which implies that oxidation of TMA by holes generated at the n/p interface efficiently occurs at the AlPcCl surface.

For the nanoparticles, the current directions of the monocomponent particles (Figure 7a,b) are the same as those of the corresponding vapor-deposited films (Figure S2a,b in the Supporting Information), respectively. The threshold potential values for the photoanodic current of the C_{60} particles and the anodic current of the AlPc particles are similar to those of the corresponding vapor-deposited monolayer electrodes, respectively (Table 1). Moreover, the nanoparticle composite exhibits a threshold potential value of −0.2 V for photoanodic current (Figure 7c), the photocurrent direction and threshold potential of which are also similar to those of the vapor-deposited ITO/C_{60}/AlPcCl (Figure S2c in the Supporting Information), respectively, in the presence of TMA. These results identify the semiconducting properties of the nanoparticles with those of the vapor-deposited films.

The photocurrent inferiority of the nanoparticle composite (Figure 7c), compared to the vapor-deposited ITO/C_{60}/AlPcCl (Figure S2c in the Supporting Information), is explained by the poor electron injection into the ITO electrode and random orientations of the particles to the base electrode (Figure 8). Considering that the vapor-deposited ITO/AlPc/C_{60} electrode does not exhibit

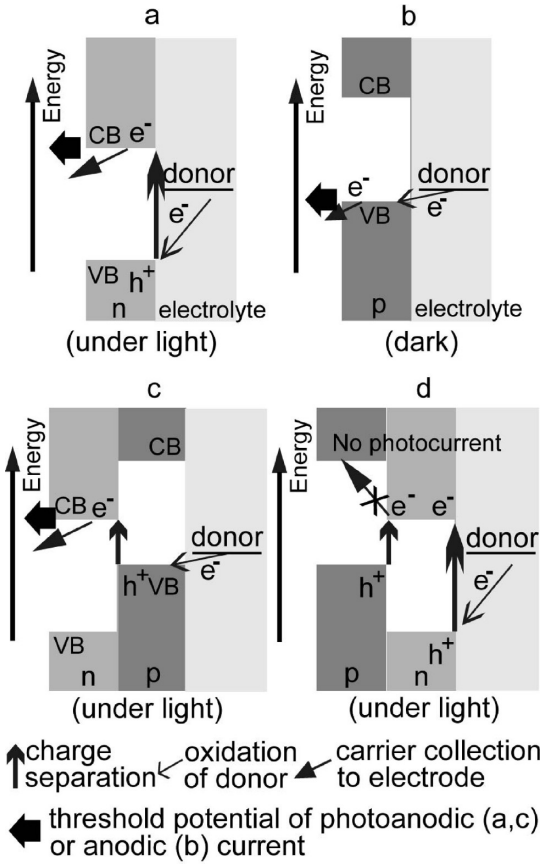

Figure 6. Schematic diagram of the photoelectrochemical processes for (a) an n-type monolayer, (b) a p-type monolayer, (c) an n/p bilayer, and (d) a p/n bilayer in the presence of an electron donor.

Table 1. Threshold Potentials for the Photoanodic Current (V_{pa}) in the Presence of TMA

	V_{pa} (V vs Ag/AgCl)	
	vapor-deposited[a]	nanoparticles[b]
ITO/C_{60}	∼−0.2	∼−0.2
ITO/AlPc	[c]	[c]
ITO/C_{60}/AlPc	∼−0.2	[d]
ITO/AlPc/C_{60}	[e]	[d]
ITO/(C_{60}/AlPc)	[d]	−0.2

[a] The values were estimated from CV data in Figure S2 in the Supporting Information. [b] The values were estimated from CV data in Figure 7. [c] The threshold potential of the anodic current was +0.4 V even in the dark. [d] The modified electrodes were not prepared. [e] The photoanodic current did not appear.

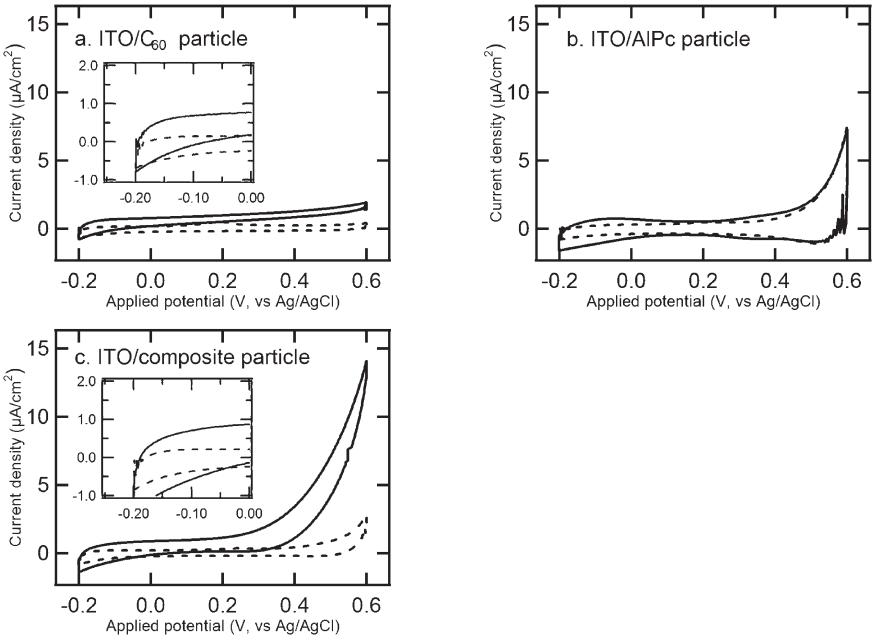

Figure 7. Cyclic voltammograms of particle films of (a) C_{60}, (b) AlPc, and (c) composite on ITO: solid line, under illumination; dashed line, in the dark. The electrolyte solution: 2×10^{-3} mol/L TMA and 0.1 mol/L KNO_3. Scan rate: 20 mV/s. Light intensity: 100 mW/cm^2. The insets of parts a and c show expansions of the −0.2 to 0.0 V region.

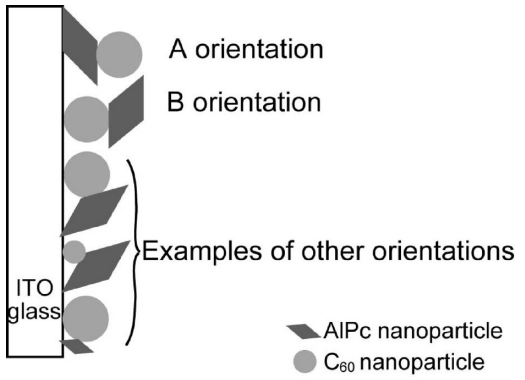

Figure 8. Schematic illustration showing the orientations of the nanoparticle composites relative to ITO.

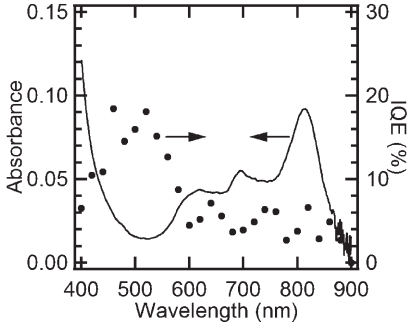

Figure 9. IQE spectrum for steady-state photoanodic current generated at an ITO/nanoparticle composite (•) and its absorption spectrum (solid line). The electrolyte solution contained 10 mmol/L TMA and 0.1 mol/L KNO_3; the applied potential was +0.55 V vs Ag/AgCl in a saturated KCl solution.

anodic or photoanodic current (Figure S2d in the Supporting Information), the photoanodic current of the nanoparticle composite would be due to nanoparticles with certain orientations relative to the ITO electrode (e.g., the B orientation in Figure 8), whereas others such as the nanoparticles with the A orientation (Figure 8) would not contribute to the photoanodic current. Despite the coexistence of random alignments, the observed photoanodic current of the composite was larger than that of the monocomponent C_{60}, similar to reported organic bilayer electrodes.[28−32] This implies that TMA oxidation by holes generated at the C_{60}/AlPc interface is more efficient than that by excitons in C_{60}.

The measurements of the absorption spectrum and incident photon-to-current efficiency enabled the calculation of the IQE spectrum shown in Figure 9, where the solid line indicates light absorption of the nanoparticle composite. The IQE spectrum also covers the full spectrum of visible light and reaches 880 nm, consistent with the absorption edge. The IQE values are variable; efficiencies of more than 10% (a maximum of about 18%) are observed at 420−560 nm and about 5% or less at longer wavelengths. The higher IQE values at 420−560 nm can be explained as follows. In the case of low absorbance, more excitons can be generated near the p/n junction; hence, the probability of exciton diffusion to the p/n junction would be higher than that in the case of large absorbance because of the shorter diffusion distance of exciton to the p/n junction.

TMA Decomposition. The photoelectrochemical behavior of the present nanoparticle composite implies similarities to organic bilayer solar cells except for the charge collection part: carrier generation in the composite is initiated by photoinduced charge separation or charge transfer from the AlPc or C_{60} excited state to the C_{60}/AlPc interface. Subsequently, electrons and holes move toward C_{60} and AlPc pieces, respectively, and reach their surface. Finally, the carriers are collected by the ITO electrode and redox process. If the nanoparticle composite is not attached to the ITO electrode, both of the carriers (electrons and holes) may be collected by redox processes without bias.

Table 2. CO_2 Generation from TMA in the Presence/Absence of Light

	produced CO_2 amount in moles (production ratio %) [a]	
catalyst	under irradiation	in the dark
C_{60}	1.1×10^{-7} (4.7)	$<0.1 \times 10^{-7}$ (<0.6)
AlPc	$<0.1 \times 10^{-7}$ (<0.6)	$<0.1 \times 10^{-7}$ (<0.6)
composite C_{60}/AlPc[b]	1.4×10^{-7} (6.3)	$<0.1 \times 10^{-7}$ (<0.6)
simply mixed C_{60}/AlPc[c]	0.6×10^{-7} (2.7)	$<0.1 \times 10^{-7}$ (<0.6)

[a] Production ratio (%) = [(amount of CO_2 produced)/(initial amount of TMA)] × 100. [b] The composite was prepared through reprecipitation from a mixed NMP solution of C_{60} and AlPcCl (0.86 mg/mL, respectively), and its loading ratio of C_{60} to AlPcCl is 4:5 in moles or 1:1 by weight. [c] Simply mixed particles were prepared by mixing the particles of C_{60} with those of AlPc (weight ratio = 1:1).

The photocatalytic activities of the resulting nanoparticles were examined in terms of oxidation of TMA to CO_2 in a heterogeneous photocatalytic test.[60−62] As shown in Table 2, the composite nanoparticles have the largest production of CO_2 among the four samples of C_{60}, AlPc, composite, and simply mixed C_{60} and AlPc under light irradiation. For the AlPc nanoparticles, the production of CO_2 is even below the detection limit. Compared to the C_{60} or simply mixed nanoparticles, the composite still has higher CO_2 production. It is noteworthy that the CO_2 generated for the simply mixed nanoparticles (0.6×10^{-7} mol) is close to the average of those for the monocomponent C_{60} (1.1×10^{-7} mol) and AlPc ($<0.1 \times 10^{-7}$ mol) nanoparticles. This result demonstrates that the C_{60}/AlPc interfaces are rarely formed by simple mixing and that TMA oxidation by holes in AlPc arising from charge separation at the C_{60}/AlPc interfaces is hardly achieved by the simply mixed sample consequently. Table 2 also shows the results without light irradiation. It is found that CO_2 generation is negligible for all of the samples. Therefore, CO_2 generation from TMA oxidation is based on light irradiation in the presence of the nanoparticles.

The descending order of CO_2 generated is very similar to that of the photoanodic current in the presence of TMA (Figure 7), where composite > C_{60} > AlPc. This suggests that the initial oxidation of TMA found in the photoanodic phenomena is the crucial process of CO_2 generation.

CONCLUSION

Nanoparticle composites composed of C_{60} and AlPc were fabricated by a wet process—reprecipitation—in which a mixed NMP solution of C_{60} and AlPcCl was injected into water. The composite has two crystalline components (C_{60} and AlPc) and responds to the full visible spectrum not only for light absorption but also for photoanodic current generation. The photoelectrochemical properties of the composite are similar to those of the vapor-deposited bilayer of C_{60} and AlPcCl with a p/n junction.

CO_2 generation from TMA decomposition by the nanoparticle composite under visible light indicates that the composite can act as a photocatalyst in the photodegradation reaction without bias potential.

■ ASSOCIATED CONTENT

Supporting Information. Elemental analysis results of composite particles (loading mole ratio of AlPcCl:C_{60} = 5:4), FTIR spectra of C_{60}, AlPc, and composite nanoparticles, and CV results of vapor-deposited films. This material is available free of charge via the Internet at http://pubs.acs.org.

■ AUTHOR INFORMATION

Corresponding Author

*E-mail: nagai.k.ae@m.titech.ac.jp. Tel: (+81) 45-924-5266. Fax: (+81) 45-924-5247.

■ ACKNOWLEDGMENT

This research was supported by the New Energy and Industrial Technology Development Organization, Tokyo Ohka Foundation, Japan, and a Grant-in-Aid for Scientific Research from the MEXT, Japan (Grant 22350099).

■ REFERENCES

(1) Tang, C. W. *Appl. Phys. Lett.* **1986**, *48*, 183–185.
(2) Wöhrle, D.; Meissner, K. *Adv. Mater.* **1991**, *3*, 129–138.
(3) Wöhrle, D.; Kreienhoop, L.; Schnurpfeil, G.; Elbe, J.; Tennigkeit, B.; Hiller, S.; Schlettwein, D. *J. Mater. Chem.* **1995**, *5*, 1819–1829.
(4) Pannemann, C.; Dyakonov, V.; Parisi, J.; Hild, O.; Wöhrle, D. *Synth. Met.* **2001**, *121*, 1585–1586.
(5) Yanagi, H.; Tamura, N.; Taira, S.; Furuta, H.; Douko, S.; Schnurpfeil, G.; Wöhrle, D. *Mol. Cryst. Liq. Cryst. Sci. Technol., Sect. A* **1995**, *267*, 435–440.
(6) Morikawa, T.; Adachi, C.; Tsutsui, T.; Saito, S. *Nippon Kagaku Kaishi* **1990**, *9*, 962–967.
(7) Hiramoto, M.; Fujiwara, H.; Yokoyama, M. *Appl. Phys. Lett.* **1991**, *58*, 1062–1064.
(8) Hiramoto, M.; Fujiwara, H.; Yokoyama, M. *J. Appl. Phys.* **1992**, *72*, 3781–3787.
(9) Peumans, P.; Uchida, S.; Forrest, S. R. *Nature* **2003**, *425*, 158–162.
(10) Fujii, A.; Shirakawa, T.; Umeda, T.; Mizukami, H.; Hashimoto, Y.; Yoshino, K. *Jpn. J. Appl. Phys.* **2004**, *43*, 5573–5576.
(11) Matsuo, Y.; Sato, Y.; Niinomi, T.; Soga, I.; Tanaka, H.; Nakamura, E. *J. Am. Chem. Soc.* **2009**, *131*, 16048–16050.
(12) Chauhan, K. V.; Sullivan, P.; Yang, J. L.; Jones, T. S. *J. Phys. Chem. C* **2010**, *114*, 3304–3308.
(13) Bottari, G.; de la Torre, G.; Guldi, D. M.; Torres, T. *Chem. Rev.* **2010**, *110*, 6768–6816 and references cited therein.
(14) Martínez-Díaz, M. V.; de la Torre, G.; Torres, T. *Chem. Commun.* **2010**, *46*, 7090–7108 and references cited therein.
(15) Hasobe, T.; Imahori, H.; Fukuzumi, S.; Kamat, P. V. *J. Phys. Chem. B* **2003**, *107*, 12105–12112.
(16) Imahori, H.; Mitamura, K.; Shibano, Y.; Umeyama, T.; Matano, Y.; Yoshida, K.; Isoda, S.; Araki, Y.; Ito, O. *J. Phys. Chem. B* **2006**, *110*, 11399–11405.
(17) Imahori, H.; Ueda, M.; Kang, S.; Hayashi, H.; Hayashi, S.; Kaji, H.; Seki, S.; Saeki, A.; Tagawa, S.; Umeyama, T.; Matano, Y.; Yoshida, K.; Isoda, S.; Shiro, M.; Tkachenko, N. V.; Lemmetyinen, H. *Chem.—Eur. J.* **2007**, *13*, 10182–10193.
(18) Kang, S.; Umeyama, T.; Ueda, M.; Matano, Y.; Hotta, H.; Yoshida., K.; Isoda, S.; Shiro, M.; Imahori, H. *Adv. Mater.* **2006**, *18*, 2549–2552.
(19) Hasobe, T.; Imahori, H.; Kamat, P. V.; Ahn, T. K.; Kim, S. K.; Kim, D.; Fujimoto, A.; Hirakawa, T.; Fukuzumi, S. *J. Am. Chem. Soc.* **2005**, *127*, 1216–1228.
(20) Kira, A.; Umeyama, T.; Matano, Y.; Yoshida, K.; Isoda, S.; Isosomppi, M.; Tkachenko, N. V.; Lemmetyinen, H.; Imahori, H. *Langmuir* **2006**, *22*, 5497–5503.
(21) Hasobe, T.; Kamat, P. V.; Absalom, M. A.; Kashiwagi, Y.; Sly, J.; Crossley, M. J.; Hosomizu, K.; Imahori, H.; Fukuzumi, S. *J. Phys. Chem. B* **2004**, *108*, 12865–12872.
(22) Ogata, T.; Hiranaga, K.; Matsuoka, S.; Wada, Y.; Yanagida, S. *Chem. Lett.* **1993**, 983–984.
(23) Wada, Y.; Ogata, T.; Hiranaga, K.; Yasuda, H.; Kitamura, T.; Murakoshi, K.; Yanagida, S. *J. Chem. Soc., Perkin Trans. 2* **1998**, 1999–2004.
(24) Wada, Y.; Kitamura, T.; Yanagida, S. *Res. Chem. Intermed.* **2000**, *26*, 153–159.
(25) Premkumar, J. R.; Ramaraj, R. *Chem. Commun.* **1997**, 343–344.
(26) Wang, X.; Maeda, K.; Thomas, A.; Takanabe, K.; Xin, G.; Carlsson, J. M.; Domen, K.; Antonietti, M. *Nat. Mater.* **2009**, *8*, 76–80.
(27) Maeda, K.; Wang, X.; Nishihara, Y.; Lu, D.; Antonietti, M.; Domen, K. *J. Phys. Chem. C* **2009**, *113*, 4940–4947.
(28) Abe, T.; Nagai, K.; Kabutomori, S.; Kaneko, M.; Tajiri, A.; Norimatsu, T. *Angew. Chem., Int. Ed.* **2006**, *45*, 2778–2781.
(29) Abe, T.; Nagai, K.; Kaneko, M.; Okubo, T.; Sekimoto, K.; Tajiri, A.; Norimatsu, T. *ChemPhysChem* **2004**, *5*, 716–720.
(30) Abe, T.; Nagai, K.; Ichinohe, H.; Shibata, T.; Tajiri, A.; Norimatsu, T. *J. Electroanal. Chem.* **2007**, *599*, 65–71.
(31) Abe, T.; Nagai, K.; Ogiwara, T.; Ogasawara, S.; Kaneko, M.; Tajiri, A.; Norimatsu, T. *J. Electroanal. Chem.* **2006**, *587*, 127–132.
(32) Abe, T.; Miyakushi, S.; Nagai, K.; Norimatsu, T. *Phys. Chem. Chem. Phys.* **2008**, *10*, 1562–1568.
(33) Abe, T.; Nagai, K.; Sekimoto, K.; Tajiri, A.; Norimatsu, T. *Electrochem. Commun.* **2005**, *7*, 1129–1132.
(34) Abe, T.; Tobinai, S.; Taira, N.; Chiba, J.; Itoh, T.; Nagai, K. *J. Phys. Chem. C* **2011**, *115*, 7701–7705.
(35) Nagai, K.; Morishita, K.; Yoshida, H.; Norimatsu, T.; Miyanaga, N.; Izawa, Y.; Yamanaka, T. *Synth. Met.* **2001**, *121*, 1445–1446.
(36) Nagai, K.; Yoshida, H.; Norimatsu, T.; Miyanaga, N.; Izawa, Y.; Yamanaka, T. *Appl. Surf. Sci.* **2002**, *197—198*, 808–813.
(37) Nagai, K.; Abe, T.; Kaneyasu, Y.; Yasuda, Y.; Kimishima, I.; Iyoda, T.; Imaya, H. *ChemSusChem* **2011**in press.
(38) Kasai, H.; Nalwa, H. S.; Oikawa, H.; Okada, S.; Matsuda, H.; Minami, N.; Kakuta, A.; Ono, K.; Mukoh, A.; Nakanishi, H. *Jpn. J. Appl. Phys.* **1992**, *31*, L1132–L1134.
(39) Tachikawa, T.; Chung, H.-R.; Masuhara, A.; Kasai, H.; Oikawa, H.; Nakanishi, H.; Fujitsuka, M.; Majima, T. *J. Am. Chem. Soc.* **2006**, *128*, 15944–15945.
(40) Tan, Z.; Masuhara, A.; Kasai, H.; Nakanishi, H.; Oikawa, H. *Jpn. J. Appl. Phys.* **2008**, *47*, 1426–1428.
(41) Kaneko, K.; Furuya, K.; Hungria, A. B.; Hernandez-Garrido, J.-C.; Midgley, P. A.; Onodera, T.; Kasai, H.; Yaguchi, Y.; Oikawa, H.; Nomura, Y.; Harada, H.; Ishihara, T.; Baba, N. *J. Electron Microsc.* **2009**, *58*, 289–294.
(42) Kasai, H.; Oikawa, H.; Okada, S.; Nakanishi, H. *Bull. Chem. Soc. Jpn.* **1998**, *71*, 2597–2601.
(43) Kasai, H.; Kamatani, H.; Okada, S.; Oikawa, H.; Matsuda, H.; Nakanishi, H. *Jpn. J. Appl. Phys.* **1996**, *35*, L221–L223.
(44) Kaneko, Y.; Onodera, T.; Kasai, H.; Okada, S.; Oikawa, H.; Nakanishi, H.; Fukuda, T.; Matsuda, H. *J. Mater. Chem.* **2005**, *15*, 253–255.
(45) Fujita, S.; Kasai, H.; Okada, S.; Oikawa, H.; Fukuda, T.; Matsuda, H.; Tripathy, S. K.; Nakanishi, H. *Jpn. J. Appl. Phys.* **1999**, *38*, L659–L661.
(46) Kasai, H.; Kanbara, H.; Iida, R.; Okada, S.; Matsuda, H.; Oikawa, H.; Nakanishi, H. *Jpn. J. Appl. Phys.* **1995**, *34*, L1208–L1210.
(47) Kwon, E.; Oikawa, H.; Kasai, H.; Nakanishi, H. *Cryst. Growth Des.* **2007**, *7*, 600–602.

(48) Partially hydrolyzed aluminum phthalocyanine chloride is referred to as AlPc; pristine aluminum phthalocyanine chloride is referred to as AlPcCl.
(49) Aksenov, V. L.; Avdeev, M. V.; Kyzyma, E. A.; Rosta, L.; Korobov, M. V. *Crystallogr. Rep.* **2007**, *52*, 479–482.
(50) Hotta, H.; Kang, S.; Umeyama, T.; Matano, Y.; Yoshida, H.; Isoda, S.; Imahori, H. *J. Phys. Chem. B* **2005**, *109*, 5700–5706.
(51) Oliveira, D.; Baba, K.; Mori, J.; Miyashita, Y.; Kasai, H.; Oikawa, H.; Nakanishi, H. *Jpn. J. Appl. Phys.* **2009**, *48*, 105003.
(52) Semenov, K. N.; Charykov, N. A.; Keskinov, V. A.; Piartman, A. K.; Blokhin, A. A.; Kopyrin, A. A. *J. Chem. Eng. Data* **2010**, *55*, 13–36.
(53) Nagai, K.; Cho, B.-R.; Hashishin, Y.; Norimatsu, T.; Yamanaka, T. *Jpn. J. Appl. Phys.* **2002**, *41*, L431–L433.
(54) Nagai, K.; Norimatsu, T.; Izawa, Y. *Fusion Sci. Technol.* **2004**, *45*, 79–83.
(55) Yevlampieva, N. P.; Biryulin, Yu. F.; Melenevskaja, E. Yu.; Zgonnik, V. N.; Rjumtsev, E. I. *Colloids Surf., A* **2002**, *209*, 167–171.
(56) Wang, L.; Liu, B.; Liu, D.; Yao, M.; Hou, Y.; Yu, S.; Cui, T.; Li, D.; Zou, G.; Iwasiewicz, A.; Sundqvist, B. *Adv. Mater.* **2006**, *18*, 1883–1888.
(57) Nisha, J. A.; Janaki, J.; Sridharan, V.; Padma, G.; Premila, M.; Radhakrishnan, T. S. *Thermochim. Acta* **1996**, *286*, 17–24.
(58) Côté, R.; Dénès, G.; Gastonguay, L.; Dodelet, J. P. *Proc. SPIE* **1992**, *1729*, 222–229.
(59) Whitlock, J. B.; Bird, G. R.; Cox, M. D.; Panayotatos, P. *Thin Solid Films* **1992**, *215*, 84–87.
(60) Hashimoto, K.; Irie, H.; Fujishima, A. *Jpn. J. Appl. Phys.* **2005**, *44*, 8269–8285.
(61) Irie, H.; Watanabe, Y.; Hashimoto, K. *J. Phys. Chem. B* **2003**, *107*, 5453–5486.
(62) Abe, R.; Takami, H.; Murakami, N.; Ohtani, B. *J. Am. Chem. Soc.* **2008**, *130*, 7780–7781.